

Contents lists available at ScienceDirect

Journal of Energy Chemistry



journal homepage: www.elsevier.com/locate/jechem

Enhancing electrochemo-mechanical properties of graphite-silicon anode in all-solid-state batteries via solvent-induced polar interactions in nitrile binders

Jaecheol Choi ^{a,b,1,*}, Cheol Bak ^{c,1}, Ju Young Kim ^{a,b}, Dong Ok Shin ^{a,b}, Seok Hun Kang ^{a,b}, Yong Min Lee ^{c,d,e,*}, Young-Gi Lee ^{a,*}

- a Smart Materials Research Section, Electronics and Telecommunications Research Institute (ETRI), 218 Gajeongno, Yuseong-gu, Daejeon 34129, Republic of Korea
- b Department of Semiconductor and Advanced Device Engineering, University of Science and Technology (UST), Daejeon 34113, Republic of Korea
- ^c Department of Energy Science & Engineering, Daegu Gyeongbuk Institute of Science and Technology (DGIST), Daegu 42988, South Korea
- ^d Department of Battery Engineering, Yonsei University, 50 Yonsei-ro, Seodaemun-gu, Seoul 03722, Republic of Korea
- ^e Department of Chemical and Biomolecular Engineering, Yonsei University, 50 Yonsei-ro, Seodaemun-gu, Seoul 03722, Republic of Korea

ARTICLE INFO

Article history: Received 2 January 2025 Revised 14 February 2025 Accepted 14 February 2025 Available online 27 February 2025

Keywords: Solid-state batteries Nitrile rubber Solvents Silicon Sulfide solid electrolytes

ABSTRACT

All-solid-state batteries (ASSBs) with sulfide-type solid electrolytes (SEs) are gaining significant attention due to their potential for the enhanced safety and energy density. In the slurry-coating process for ASSBs, nitrile rubber (NBR) is primarily used as a binder due to its moderate solubility in non-polar solvents, which exhibites minimal chemical reactivity with sulfide SEs. However, the NBR binder, composed of butadiene and acrylonitrile units with differing polarities, exhibits different chemical compatibility depending on the subtle differences in polarity of solvents. Herein, we systematically demonstrate how the chemical compatibility of solvents with the NBR binder influences the performance of ASSBs. Anisole is found to activate the acrylonitrile units, inducing an elongated polymer chain configuration in the binder solution, which gives an opportunity to strongly interact with the solid components of the electrode and the current collector. Consequently, selecting anisole as a solvent for the NBR binder enables the fabrication of a mechanically robust graphite-silicon anode, allowing ASSBs to operate at a lower stacking pressure of 16 MPa. This approach achieves an initial capacity of 480 mAh g⁻¹, significantly higher than the 390 mAh g⁻¹ achieved with the NBR/toluene binder that has less chemical compatibility. Furthermore, internal stress variations during battery operation are monitored, revealing that the enhanced mechanical properties, achieved through acrylonitrile activation, effectively mitigate internal stress in the graphite/silicon composite anode.

© 2025 The Authors. Published by Published by Elsevier B.V. and Science Press on behalf of Science Press and Dalian Institute of Chemical Physics, Chinese Academy of Sciences. This is an open access article under the CC BY license (http://creativecommons.org/licenses/by/4.0/).

1. Introduction

Lithium-ion batteries (LIBs) have gained widespread recognition as one of the most promising power sources, driving a shift from non-renewable fossil fuels to renewable energy solutions [1,2]. This transformation is evident in the replacement of internal combustion vehicles with electric vehicles (EVs). Over the past decade, the global market share of EVs has steadily increased, while that of petrol vehicles has seen a significant decline. Despite the

growing adoption of EVs, the industry still faces several challenges, including safety, driving range, and charging infrastructure. Among these, safety is regarded as the most critical issue, primarily due to the use of flammable and volatile liquid electrolytes (LEs) in LIBs. While LEs offer high ionic conductivity and their liquid state enables efficient ionic conduction within the complex porous structure of electrodes, the organic carbonate-based electrolytes pose significant safety risks. These electrolytes can ignite or even explode in emergency situations, making them the greatest concern in LE-based LIB systems [3–5].

Recently, it is widely believed that replacing liquid-formed electrolyte with thermally stable solid-state electrolyte can mitigate the safety issues possessed in LE-based LIBs and the energy density of batteries could be potentially maximized by

^{*} Corresponding authors.

E-mail addresses: jaecheol.choi@etri.re.kr (J. Choi), yongmin@yonsei.ac.kr (Y.M. Lee), lyg@etri.re.kr (Y.-G. Lee).

¹ These authors contributed equally to this work.

designing bipolar-stacked electrode [6-10]. Furthermore, sulfidetype solid electrolyte (SE) has shown a fast lithium ion conductivity comparable to the liquid electrolyte ($>10^{-3}$ S cm⁻¹ within the polyethylene separator) and also, they exhibited a low Young's modulus at ~20 GPa, leading to the formation of intimate surface contact between solid particles [11-13]. Even though sulfidetype solid electrolyte is considered as a promising SE candidate for all-solid-state batteries (ASSBs), the chemical form of argyrodite (PS_4^{3-}), the main component of sulfide electrolyte, is very unstable to the moisture in the atmosphere, leading to decomposition into a toxic H₂S gas with decreasing Li⁺ conductivity [9]. Regarding the instability of sulfide SEs, this leads to another issue in terms of the scalable production. For now, ASSBs have been mainly studied by pelletizing the solid components (active materials, solid electrolyte, and conductive agents) and the pelletized electrodes with a thickness of a few hundred micrometers are generally used for the study of the solid-solid interfacial reactions between particles [14,15]. Considering a practical point of view in the scalable production of batteries, however, solvent-based processes like a wet slurry casting method, which is utilized in the traditional manufacturing process in LIBs, are necessary for roll-to-roll electrode manufacturing process [16–20]. Nonetheless, the poor chemical stability of sulfide SEs is limiting the uses of polar solvents (e.g. N-methyl-2-pyrrolidone and H₂O), and nonpolar solvents (e.g. xylene and toluene) are widely adopted to dissolve binder or adjust a viscosity of electrode/SE slurry for the studies of wet-process ASSBs [16,21]. However, solvents like toluene and xylene (including their meta-, ortho-, and paraisomers) exhibit weak intermolecular forces [22], resulting in rapid evaporation during slurry preparation. This evaporation rate is also particularly accelerated under low-humidity conditions, such as those found in glove boxes or dry rooms, which are commonly used in the processing of sulfide SEs [23,24].

For the binder materials used in wet-slurry casting, nitrile rubber (NBR) binders, dissolved in solvents such as xylene or toluene, are commonly used due to their minimal reactivity with sulfide SEs in sulfide-type ASSBS [25,26]. NBR is a copolymer consisting of two distinct monomers, butadiene and acrylonitrile, with contrasting polarities [20]. While butadiene is non-polar, the nitrile group in acrylonitrile exhibits strong polarity, making it theoretically incompatible with non-polar solvents. This incompatibility leads to only partial dissolution of NBR in solvents such as toluene or xylene. Consequently, these solvents make it more difficult to fully exploit the co-polymeric nature of NBR, limiting the inherent properties of both butadiene and acrylonitrile. In particular, polar functionalities, such as the nitrile groups in acrylonitrile, could possibly enhance mechanical properties by interacting with surface functionalities on the solid particles within the electrode [27,28].

To validate the use of proper solvents for dissolving NBR binders, Lee et al. reported the reactivity of sulfide SEs with various solvents and demonstrated that para-xylene (p-xylene) does not affect the crystal structure of sulfide SEs. They concluded that pxylene is an appropriate solvent for processing NBR binders in ASSBs [21]. Additionally, Kim et al. investigated a co-solvent system comprising dibromomethane and hexyl butyrate. This system successfully modulated the solubility of LiTFSI and NBR copolymers, enabling the development of a wet-processable Li⁺ conductive binder solution for sulfide-type ASSBs. In their study, various compositions of co-solvent mixtures were tested to evaluate the solubility of NBR and Li salt as well as the reactivity with Li₆PS₅Cl (LPSCI) [16]. However, the co-polymeric nature of NBR, which influences its solubility in solvents, was not carefully considered in the selection of solvent. Regarding the acrylonitrile units in the NBR binder, Lee et al. studied how the acrylonitrile content in the NBR binder influences sulfide-type ASSB performance. All binders in their study were dissolved in a co-solvent system of *N*-butyl butyrate and benzyl acetate. They found that acrylonitrile with a moderate content (25 wt%) enhanced the mechanical properties of the cathode electrode, resulting in the improved cycle performance [29]. Although the study showed better battery performance using an NBR binder containing 25% of acrylonitrile, it also did not thoroughly address the compatibility between solvents and the individual components of the NBR copolymer.

In this study, three solvents with subtly varying polarities, such as toluene, p-xylene, and anisole, were utilized to dissolve the NBR copolymeric binder for wet-processable ASSBs. The results revealed that anisole, with its methoxy substituent, exhibited slightly higher polarity than toluene or p-xylene, making it more compatible with the acrylonitrile units in the NBR binder, leading to better solubility of the binder in anisole. This enhanced solubility was attributed to the interaction between anisole and acrylonitrile units, which led to the activation of dipole-dipole interactions between the particles and/or the current collector, enhancing the mechanical properties of the binder. The improved mechanical properties of the NBR/anisole binder system were effectively applied to a graphite/silicon anode for ASSBs, operating under a pressure of 48 MPa, and this system restricted volume expansion during the charge-discharge process, leading to the enhanced battery performance. Additionally, the enhanced mechanical properties allowed the electrode to operate at reduced stacking pressure of 16 MPa by alleviating internal stress, further improving performance. Therefore, this work demonstrates that the compatibility between solvent and polymeric binder must be carefully considered based on their molecular structures and chemical properties, and this work also offers a potential solution for reducing the operating pressure of ASSBs.

2. Experimental

2.1. Materials

The commercial nitrile butadiene rubber (NBR, $Mv \sim 80$ k, nitrile content $\sim 32\%$) and polybutadiene (PB, $Mw \sim 200$ k) were supplied by LG Chem and Sigma aldrich korea, respectively. Solvents of anisole, toluene, and p-xylene were purchased by Sigma aldrich korea and used without any purification. Natural graphite was supplied by POSCO Future M in Korea and silicon nanoparticles (30–50 nm) were purchased from Alfa-aesar in USA. Li₆PS₅Cl solid electrolyte (LPSCl, average particle size ~ 3 µm, ionic conductivity ~ 3 mS cm $^{-1}$) was purchased from Posco JK Solid Solution in Korea. Lithium metal (thickness ~ 300 µm) was purchased from Honjo metal in Japan. It is important to note that all chemicals used in this work are consistently stored in a dry room where the dew point was maintained consistently below -60 °C. Consequently, any moisture absorbed/adsorbed on the chemicals is likely to desorb before use.

2.2. Preparation of sheet-type graphite/silicon composite electrode

The graphite/silicon anode slurry was prepared by mixing 70 wt% active materials (NG:Si = 90:10 wt%), 26 wt% LPSCl, and 4 wt% NBR dissolved in anisole, and toluene or p-xylene with a planatery mixer (Thinky corp., ARM-310). The viscosity of slurry was adjusted by additional solvents (anisole, toluene, or p-xylene, depending on the solvent used for preparation of NBR solution) and the homogeneously dispersed slurry was obtained. The prepared slurry was subsequently coated onto Ni foil (10 μm , Nipon steel, Japan) and dried in a convection oven at 120 °C for 30 min. The mass loading of graphite/silicon was controlled at 3.1 mg cm $^{-2}$ (For pressure monitoring experiment, the electrode loading was adjusted to 1.8 mg cm $^{-2}$). All procedures were

performed in a dry room with a dew point of -60 °C. For the preparation of LPSCI electrode to measure ionic conductivity as a function of solvents, a same procedure that was used for anode electrode preparation was adopted, but the weight ratio of electrode was fixed to LPSCI/NBR (dissolved in anisole, toluene, or p-xylene) of 98/2 (wt%).

2.3. Cell assembly and evaluation of all solid-state batteries

To prepare a layer (or membrane) of solid electrolyte (SE), ~150 mg of LPSCl powder was pelletized in a home-made polyether ether ketone mold using a hydraulic uniaxial press at 480 MPa. Graphite/silicon electrode was placed on one side of the pelletized SE layer and cold pressed at 480 MPa and then Li metal was placed on the other side of pelletized SE layer to form a lithium metal half-cell. All cells were tested under constant stacking pressure of 48 MPa. Prior to electrochemical performance tests, all cells were sealed with Al pouch to avoid exposure to humid air. For battery evaluation, cells were first charged/discharged at 0.15 C in the potential range of 0.01-2 V for 3 cycles as formation step. After then, the cells were charged and discharged at 0.15, 0.3, 0.75, and 1.5 C for 3 cycles each to evaluate rate capability, followed by testing the cycle life at 0.3 C for 100 cycles. All cells underwent charging to 0.01 V using constant current and constant voltage (cut-off: 10% current) modes, followed by discharging to 2 V via constant current mode.

For the analysis of electrochemical behavior, cyclic voltammetric (CV) analysis was performed at 60 °C with a scan rate of 0.2 mV s⁻¹ in the same potential range applied for battery test. Impedance analysis was performed to obtain ionic conductivities of LPSCl pellet/films or observe resistance changes after cycling in amplitude of 10 mV between frequencies of 5×10^{-2} – 10^6 Hz with Biologics SP-150.

The ionic conductivity of LPSCl pellet/films was calculated using the formula of σ = l/($R \times A$), where σ is the ionic conductivity (S cm⁻¹), l is the thickness of LPSCl pellet or films (cm), A is the electrode area (cm²), and the $R(\Omega)$ is the bulk resistance of the LPSCl pellet or films used in this work.

2.4. Characterizations

Polymer domain size analysis was carried out using Dynamic Light Scattering method (ELSZ-2000, Otsuka Electronics Co., Ltd). X-ray diffraction (XRD) analysis on the LPSCI SE was conducted by using an X-ray diffractometer (Empyrean, Malvern Panalytical) equipped with Cu $K_{\alpha 1}$ radiation (λ = 1.540598 Å), measured in the 2θ range of 10° – 70° . In order to suppress exposure to moisture in the air, the LPSCI samples were placed on a special sampling holder and the LPSCI samples were covered with a polyimide film. All sampling procedures were carried out in a dry room. Scanning electron microscopy (SEM, SEC SNE-4500 M) and energy-dispersive X-ray spectroscopy (EDS, Bruker XFlash 640H Mini) were utilized to analyze the morphological structure and elemental mapping, respectively.

Peel strength measurement was carried out using a 180° peel test machine with a testing speed of $0.50~\rm mm~s^{-1}$. For the analysis of pore ratio on the LPSCI films, image J software was used for processing the images obtained from SEM. Adhesion strength of the electrode was analyzed by peel tester (TXA, Yeonjin S-tech) and surface and interfacial cutting analysis system (SAICAS, SAICAS-DN-EX, Daipla Wintes, Japan). The measurements were performed with a boron nitride blade, which has the width of 1 mm and shear, rake, and clearance angles of 45° , 20° , and 10° , respectively. Interfacial adhesion between the electrode layer and current collector was measured under constant load mode (a cutting load of $0.5~\rm N$ and a peeling load of $0.2~\rm N$). Cohesion within the electrode layer

was determined at a mid-depth (i.e., 50% of the distance between the electrode surface and interface). The cohesion was measured under constant velocity mode using the same boron nitride blade, which was moved horizontally and vertically at velocities of 2.0 μ m and 0.2 μ m s⁻¹, respectively, to reach target depth positions. And then, the measurement was performed by moving the blade horizontally at a velocity of 2.0 μ m s⁻¹. Each measurement was repeated at least three times for each sample to ensure the reliability of the results. The charge/discharge properties of the ASSBs were measured using a cycle tester (Toyo System) at 60 °C.

3. Results and discussion

To examine the compatibility between the polymeric binder and solvents. NBR was selected as the primary polymeric binder in this work, as illustrated in Fig. 1(a). NBR binder solutions were prepared by dissolving the binder in three different solvents: anisole, toluene, and p-xylene. The molecular structure of the NBR copolymer comprises two distinct building blocks, butadiene, and acrylonitrile, each with contrasting chemical polarities. While butadiene is non-polar, acrylonitrile contains nitrile groups with strong polarity. Due to these different properties, the solubility of NBR is expected to vary depending on solvent polarity. However, despite the low polarity of toluene and p-xylene, numerous previous studies have reported their use for dissolving NBR binder materials [16,21]. This preference is primarily due to the negligible reactivity of these solvents with sulfide solid electrolytes. Nevertheless, the low polarity of toluene and p-xylene poses challenges in dissolving the polar acrylonitrile units in the NBR binder, leading to incomplete dissolution and less homogeneous binder solutions. In contrast, anisole, with its methoxy group substituted on the benzene ring, exhibits increased polarity, as illustrated by the molecular electrostatic potential shown in Fig. S1, where the red colored regions indicate electron-dense areas with partial negative

The effect of solvent polarity on NBR solubility was visually demonstrated through photographs of NBR dissolved in different solvents (Fig. 1b). As the solvent polarity increased from p-xylene to anisole, NBR solubility was improved significantly, with the solutions becoming more transparent and viscous. In contrast, as mentioned earlier, NBR solutions in toluene and p-xylene appeared opaque, and agglomerates of NBR were observed. Over time, these agglomerates settled at the bottom of the vials, highlighting the poor solubility of NBR in these solvents. It is important to note that the solubility of the NBR copolymer was limited, even at 80 °C, and agglomerates of NBR were still observed, as shown in Fig. S2. This suggests a limitation in the compatibility between the solvent and NBR, particularly with the nitrile group. To further investigate the significance of the molecular polarity of the solvent, we also tested ortho-xylene (o-xylene), which has methyl groups at the 1 and 2 positions on the aromatic benzene ring, to determine its effect on NBR solubility (Fig. S3). As shown in Fig. S4, the solution became more transparent and viscous compared to p-xylene, suggesting that the nitrile groups were more effectively activated by the methyl groups at the 1,2-positions in o-xylene. While the polymer solution in o-xylene showed increased transparency and viscosity, the interaction between the methyl groups and acrylonitrile groups in the NBR copolymer may still be weak, leading to inferior mechanical properties of the electrode. These observations underscore the crucial role of solvent polarity in determining the solubility of NBR binder materials, which can directly influence the physical properties of the resulting binder solution.

To further investigate the microstructural evolution of NBR in different solvent systems, dynamic light scattering (DLS) analysis was conducted on NBR samples dissolved in anisole, toluene, and

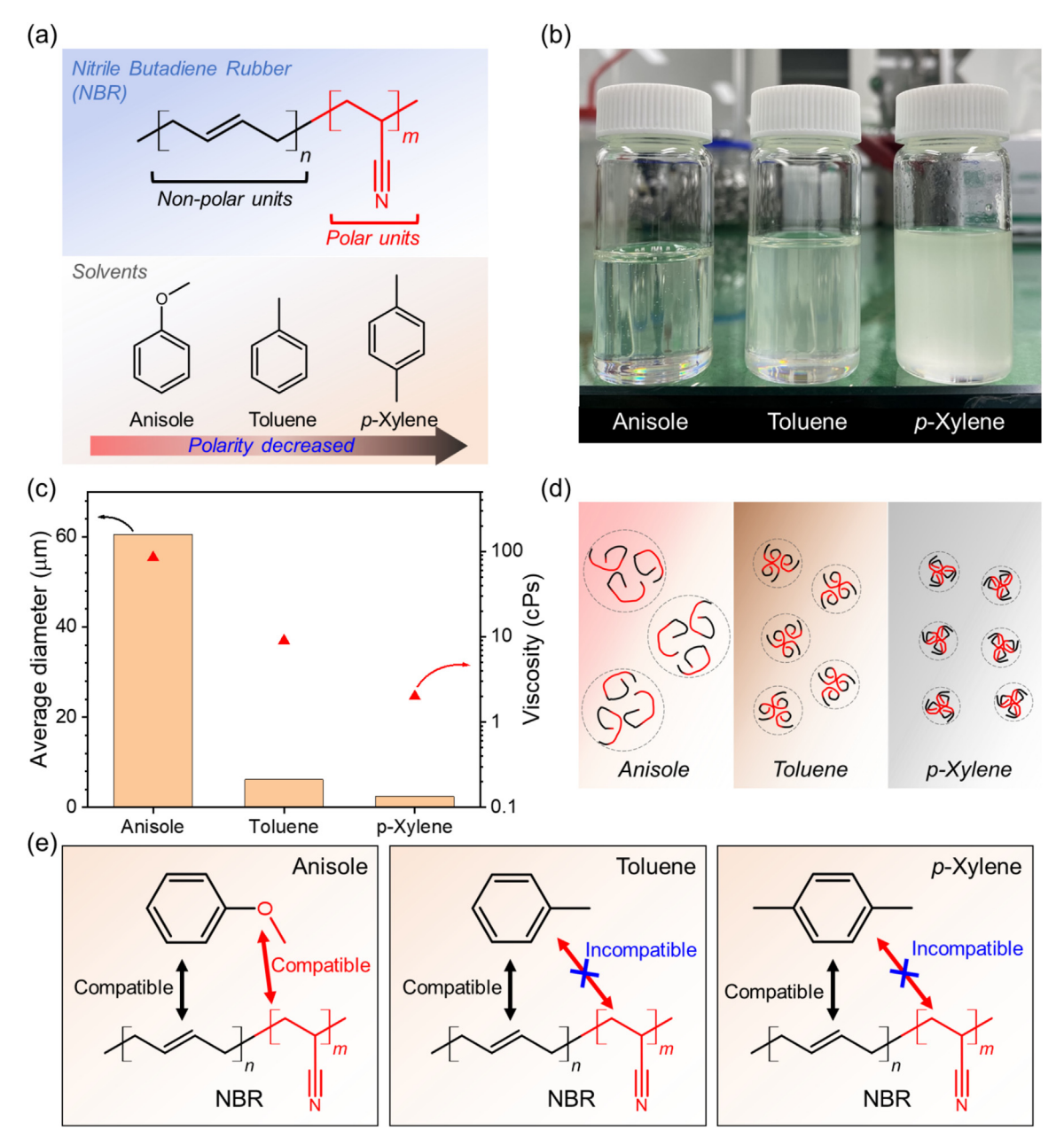


Fig. 1. (a) Molecular structure of NBR copolymer and solvents (anisole, toluene, and p-xylene). (b) Photographs of binder solutions dissolved in different solvents (from left to right: anisole, toluene, and p-xylene). (c) Results of polymeric domain size analysis and viscosity of each binder solution. (d) Illustration of polymeric domains in different solvents. (e) Molecular compatibility between each unit of NBR copolymer and solvents (anisole, toluene, and p-xylene).

p-xylene, respectively (Fig. 1c and Fig. S5). As expected, NBR dissolved in anisole (NBR-A) exhibited an average particle size of 61 µm, whereas significantly smaller domains were observed for NBR/toluene (NBR-T) and NBR/p-xylene (NBR-X) solutions, with particle sizes of 5 and 2.5 µm, respectively (left y-axis in Fig. 1c). The decreasing domain size of the polymer correlated with the decreasing viscosity of the binder solutions, which were measured to be 85, 10, and 2 cPs for NBR-A, NBR-T, and NBR-X, respectively (right y-axis in Fig. 1c). This correlation suggests that the polymeric structure of NBR exhibits a strong affinity with the polar anisole solvent, as evidenced by the larger polymeric binder domains observed in the DLS measurements [16,30]. In contrast, the polymer domains of NBR dissolved in toluene and p-xylene were significantly smaller compared to those in anisole, and it is expected that the microstructure of NBR in toluene and p-xylene is likely to consist of agglomerates, where acrylonitrile units form a compact core surrounded by butadiene chains that interact weakly with

the solvent (Fig. 1d). Therefore, this finding implies that the acrylonitrile units in NBR interact with the methoxy substituents in anisole, facilitating the enhanced solubility, while the molecular polarity of toluene and p-xylene solvents is not high enough to activate the acrylonitrile groups in NBR, leading to lower solubility in these solvents (Fig. 1e).

The behavior of polymeric domain formation in different cosolvents for the application of ASSBs has also been previously investigated, particularly in relation to Li⁺ transfer in the composite electrode [16]. It has been suggested that a smaller polymer domain formed in the composite electrode would help secure the Li⁺ pathway by minimizing the coverage ratio of interparticle interfaces. When considering the intrinsic properties of each monomer unit in the co-polymer structure, however, a partially dissolved polymer solution, which forms smaller polymer domains, may restrict the role of the co-polymer binder in the electrode fabrication process and battery operation. In particular, the

acrylonitrile units in the NBR binder have been known to enhance mechanical properties by forming dipole interactions between the highly polar nitrile groups and the SE, active materials, or current collectors. Therefore, selecting the appropriate solvent to dissolve the NBR binder becomes a crucial factor in exploiting an intrinsic properties of polymer and this also ensures the mechanical properties of the battery electrode.

Primarily, the chemical compatibility between LPSCl and solvents (p-xylene, toluene, and anisole) was investigated by analyzing the crystal structure and morphological properties of LPSCI after exposure to different solvents. For the preparation of solvent-exposed LPSCl particles, 1 g of LPSCl was added to 10 mL of each solvent, and the dispersion was vigorously mixed using a vortex mixer for 10 min. The resulting dispersion was then centrifuged, and the supernatant was removed. Prior to crystal structural analysis, the residual LPSCI particles were fully dried in a vacuum at 60 °C overnight. As shown in the XRD analysis results. the LPSCI exposed to the three different solvents showed diffraction patterns identical to those of the pristine LPSCI particles (Fig. S6). Additionally, the morphological properties of LPSCI, observed via SEM, did not change during the solvent exposure step (Fig. S7). These findings indicate that the solvents used for dissolving NBR in this study do not chemically react with the LPSCI

To investigate the effect of polymeric domain forms on the ionic conductivity in the LPSCI SE, LPSCI films were prepared using the slurry casting method with NBR dissolved in different solvents, in a composition of LPSC1: binder = 98:2 (wt%). Before analyzing the ionic conductivity, the surface morphologies of each film, densified under a pressure of 480 MPa, were observed by SEM. All films exhibited similar surface morphologies, with negligible differences in the surface pore ratio: 0.35%, 0.85%, and 1.5% for NBR-A, NBR-T, and NBR-X, respectively (white points/regions in Fig. S8d-f). For the ionic conductivity analysis of each film, the prepared LPSCl films were used to fabricate symmetric cells for electrochemical impedance spectroscopy (EIS) measurements. As shown in Figs. S9 and S10, the ionic conductivity of the pelletized LPSCI was measured to be 2.1 mS cm⁻¹. In contrast, the ionic conductivity of the LPSCl films prepared by the slurry casting method decreased more than two-fold, with measurements of 0.69 mS cm⁻¹ (anisole), 0.77 mS cm⁻¹ (toluene), and 0.74 mS cm⁻¹ (p-xylene) under the same external pressure of 480 MPa (Table S1). This result may be in line with the previous reports [16,21], which described that the forms of swollen polymer domains in the electrode were significantly influencing the formation of Li⁺ pathway. In case of LPSCl film prepared with NBR/anisole binder in this work, a lower ionic conductivity was observed and this was likely due to the increased SE coverage ratio by large size of polymer domain, compared to NBR-T and NBR-X [31]. Another possibility is that the methoxy unit in the anisole solvent could activate the nitrile groups in the NBR binder, leading to the formation of activated nitrile groups. As shown in our previous work [20], these nitrile groups can decompose upon reacting with LPSCl in either chemical or electrochemical reactions. This could result in the formation of passivating layers on the LPSCI powder when in contact with the nitrile group of the NBR binder, which would further decrease ionic conductivity (Fig. S11).

To confirm whether the selection of solvent for dissolving the acrylonitrile units in the NBR binder affects the mechanical properties of the electrode, electrodes composed of active materials (natural graphite (NG, \sim 16 μ m): silicon (Si, \sim 50 nm) = 90:10 by weight), LPSCl, and binder (NBR-A, NBR-T, and NBR-X) were fabricated with a weight ratio of 70:26:4. The composite electrodes were cold-pressed at 480 MPa, and the surface morphologies of the electrodes were analyzed by SEM. As shown in Fig. 2(a–c), NG (black circular shapes), Si, and LPSCl (grey-colored region) were

uniformly distributed throughout all the electrodes, regardless of the solvent used to dissolve the NBR binder. The distribution of each particle in the electrode was also confirmed by the EDS mapping results shown in Fig. \$12.

The composite electrodes prepared using NBR binders dissolved in different solvents were subjected to surface and interfacial cutting analysis system (SAICAS, SAICAS-DN-EX, Daipla Wintes, Japan) analysis to determine whether the activation of acrylonitrile units in NBR by the relatively polar anisole solvent affects the mechanical properties of the composite electrodes. SAICAS analysis was carried out using two different cutting modes: a constant load mode to assess the adhesion between the electrode coating layer and the Ni substrate, and a constant velocity mode to evaluate the cohesion among electrode particles (e.g., active materials and LPSCI) (Fig. 2d and Fig. S13) [32-34]. For adhesion analysis, the electrode containing NBR-A exhibited the strongest adhesion, with a value of 245 N m⁻¹, compared to 214 N m⁻¹ for NBR-T and 197 N m⁻¹ for NBR-X (Fig. 2e). Additionally, cohesion properties, measured by cutting through the mid-depth of the coating layer, showed also significant variation depending on the binder system (Fig. 2f). The NBR-A showed a cohesion strength of approximately 187 N m⁻¹, whereas the NBR-T and NBR-X systems exhibited much lower values of around 93 and 65 N m⁻¹, respectively. According to the results of measurement of cohesion and adhesion in this system, the mid-depth cohesion strength was noticeably lower than the adhesion strength at the interface between the electrode layer and the current collector. The sample thickness for SAICAS analysis was approximately 20 µm (Fig. S13), which is comparable to the particle size of graphite (16 µm) used in this study. This implies that a single layer of graphite was likely loaded onto the current collector. Furthermore, considering the density of active materials (\sim 2.2 g cm⁻³) and LPSCl (\sim 1.7 g cm⁻³), the volume ratio of active materials/LPSCl could be calculated to be 68/32, indicative of high volume of solid electrolyte in the electrode layer (Fig. S14). Given the particle size of graphite, the NBR binder in the mid-depth region primarily interacts with the graphite active material. Based on Fourier-transform infrared spectroscopic analysis of the graphite particles (Fig. S15), it was found that the graphite surface has an insufficient number of functional groups, such as hydroxyl and carboxyl groups, leading to weak dipole interactions with the NBR binder. As shown in Fig. S16, the NG electrode containing 2 wt% NBR-A exhibited a significantly lower peeling strength compared to that measured with LPSCl electrode. This suggests that the NBR-A binder is more compatible with LPSCl powder than that with NG powder in the electrode. Therefore, in the interface region, a larger volume of the current collector and LPSCl is in contact with the NBR binder, which may contribute to the enhanced adhesion strength (Fig. S17). This result suggests that acrylonitrile, when activated by the anisole solvent, helps establish a bond between solid particles and the Ni substrate. As summarized in Fig. 2(g), anisole-induced activated acrylonitrile units help bond both the current collector and electrode particles together, while the NBR-T and NBR-X systems were less effective in this regard, resulting in weaker adhesion/cohesion strength in the electrode (Fig. 2h).

To confirm the polar interaction between acrylonitrile units and other electrode components, a 180° peel-off analysis was also performed using electrodes fabricated with polybutadiene (PB), which consists solely of butadiene units, as the control binder material (Fig. S18). This confirmed that the composite electrode with a PB binder exhibited notably weak adhesion properties, with a peel strength of 1.4 N m⁻¹, suggesting that the non-polar butadiene units do not contribute to enhancing the mechanical properties of the composite electrode. For the electrodes fabricated with NBR binders containing acrylonitrile units, in contrast, the mechanical properties of each electrode were significantly improved, with average peel strengths of 278, 86, and 23 N m⁻¹

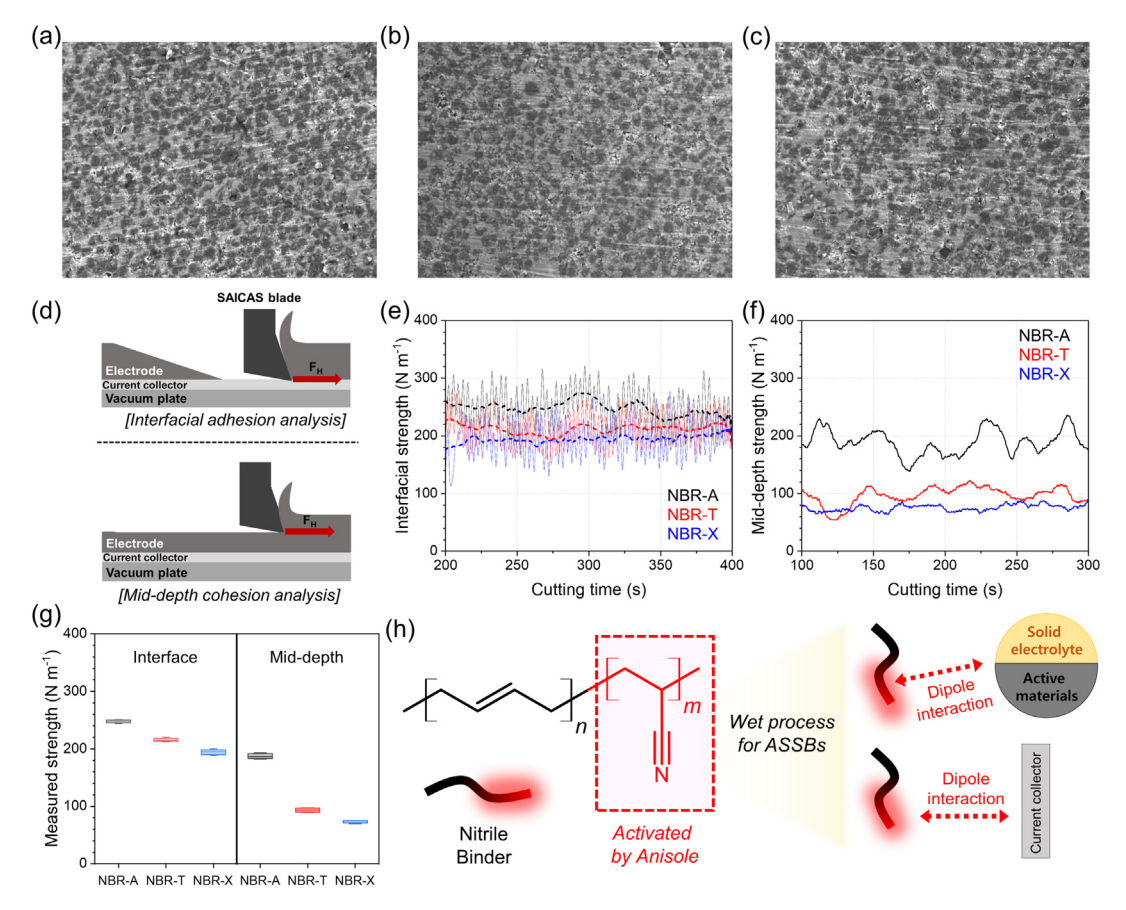


Fig. 2. (a-c) Surface morphological analysis of NBR-A, NBR-T, and NBR-X electrodes. (d) Illustration of SAICAS analysis for the measurement of interfacial adhesion force (up) and mid-depth cohesion force in the electrode (down). SAICAS results for analysis of (e) interfacial adhesion and (f) mid-depth cohesion forces on the graphite/silicon electrodes composed of NBR-A, NBR-T, and NBR-X, respectively, and (g) their summary chart. (h) Binding mechanism of NBR copolymer binder with active materials, solid electrolyte, and current collector.

for NBR-A, NBR-T, and NBR-X, respectively. These results indicate that the acrylonitrile units in the NBR binder clearly act as interaction sites, forming dipole interactions between the highly electronegative nitrogen (N) of the nitrile group and other components in the composite electrode.

For the battery performance of each composite electrode with different binders, NG/Si composite electrodes and Li metal were used to fabricate a lithium metal half-cell with a pelletized LPSCl electrolyte layer. A stack pressure of 48 MPa was applied during battery operation. Prior to measuring battery performance, the electrochemical behavior of each composite electrode was analyzed by performing CV at a scan rate of 0.2 mV s⁻¹ in a chamber temperature maintained at 60 °C. As shown in Fig. S19, the cyclic voltammograms obtained from the three different binder systems exhibited similar electrochemical behaviors, with no distinct side reactions. This indicates that the NBR binder present in the composite electrodes was not electrochemically reactive in the operating potential for anode. At the first electrochemical lithiation potential (0.01 V vs. Li^{+/0}) of the NBR-A electrode, the current density was 4.4 mA cm⁻², decreasing to 3.1 mA cm⁻² in the subsequent cycle. This 29% if loss in lithiation kinetics is attributed to electrode structural deformation caused by silicon pulverization during the first cycle and the formation of a resistive solid electrolyte interphase (SEI) layer on the active materials. In comparison, the NBR-T and NBR-X electrodes showed more significant reductions in lithiation rate, with losses of 40% and 42%, respectively, by the second cycle. This suggests that the activation of nitrile groups by the anisole solvent may enhance the mechanical properties of the NBR-A electrode, improving its electrochemical performance. Additionally, the stability of NBR binder systems was evaluated

by interfacing them directly with metallic lithium. To analyze the stability of the binder against lithium metal, we performed EIS analysis on symmetric cells both in their as-prepared state and after 10 h. Similar to the results without an interlayer (Fig. S20), all cells with LPSCI interlayers containing binder materials showed either no change or only a minimal increase in resistance after 10 h compared to the fresh samples. These results confirm that the binder system used in this study is suitable for operation at potentials down to metallic Li.

Battery performance was also tested with a current density of 0.31 mA cm⁻² (0.15 C-rate) at an operating temperature of 60 °C, and each electrode showed slightly different electrochemical properties, particularly in capacity (Fig. 3a-c). For all half-cells tested, the initial charge/discharge capacities appeared to depend on the adhesion strengths of the electrodes. For the NBR-A electrode, the initial discharge capacity was 510 mAh g⁻¹, while the NBR-T and NBR-X electrodes showed capacities of 469 and 464 mAh g⁻¹, respectively. Based on our previous studies [34,35], the practical capacities of graphite and silicon used in this work are approximately 370 and 1700 mAh $\rm g^{-1}$, respectively (as summarized in Table S2), and the observed capacity values in this study are consistent with the theoretical value of ~504 mAh g⁻¹ for a 90 wt% NG + 10 wt% Si mixture. Additionally, it has been confirmed that the binder content in the electrode does not influence the capacity contribution from either the graphite or silicon materials (Fig. S21).

Although the typical electrochemical peaks of graphite and silicon in the charge-discharge process likely overlapped due to their similar reaction potential ranges for lithiation and de-lithiation, the capacity contribution of graphite and silicon to the total

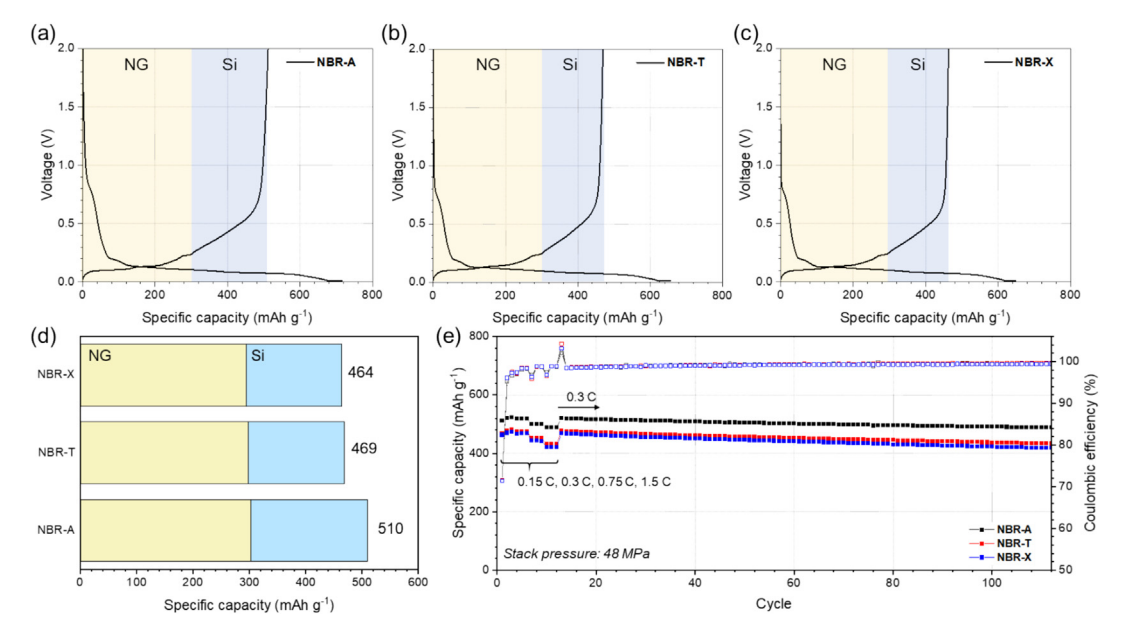


Fig. 3. (a–c) Charge-discharge voltage profiles of all solid-state NG-Si electrodes employing (a) NBR-A, (b) NBR-T, and (c) NBR-X binder at operating temperature of 60 °C. (d) Discharge capacity from each electrode containing three different binders (NBR-A, NBR-T, and NBR-X) and their capacity contribution from NG and Si. (e) Rate capability at 0.15, 0.3, 0.75, and 1.5C and consecutive cycle test for 100 cycles at 0.3C (Filled symbols: capacity, Empty symbols: coulombic efficiency). All results in this figure were obtained at a fixed stacking pressure at 48 MPa with operating temperature of 60 °C.

capacity can be approximately divided based on the plateau of NG or Si observed in the voltage profiles, as shaded with different colors in Fig. 3(a–c) (light yellow: NG, light blue: Si). As summarized in Fig. 3(d), all electrodes exhibited a similar discharge capacity of ~285 mAh g $^{-1}$ from NG, while the discharge capacities from Si varied depending on the adhesion strength of each electrode (NBR-A: 224 mAh g $^{-1}$, NBR-T: 188 mAh g $^{-1}$, and NBR-X: 183 mAh g $^{-1}$). This suggests that the enhanced mechanical properties of the NBR-A binder can effectively alleviate electrode structural damage caused by the volume expansion of Si, leading to increased capacity during the charge-discharge process.

To further investigate battery performance, composite electrodes with different binder systems were evaluated at various C-rates of 0.15, 0.3, 0.75, and 1.5 C for 3 cycles each. The NBR-A electrode showed approximately 93% of capacity retention at 1.5 C, compared to that obtained at 0.15 C, while the capacity retention for the NBR-T and NBR-X electrodes was 90% and 89%, respectively, under the same conditions. Following the rate capability test, cyclability was also evaluated at 0.3 C for 100 cycles. In terms of cycle performance, the NBR-A electrode exhibited the highest capacity retention of 94% after 100 cycles, while the NBR-T and NBR-X electrodes showed 91% and 89% of capacity retention, respectively. EIS was conducted to assess the evolution of resistance after cycling tests. As shown in Fig. S22, the first semicircle observed at high-mid frequencies in the NBR-A cell was significantly smaller compared to that in the NBR-T and NBR-X cells. This suggests that the mechanical properties of the NBR-T and NBR-X binders were insufficient to maintain the interfaces in the electrode over 100 cycles, leading to an increase in interfacial resistance and poorer capacity retention.

The tested cells were disassembled, and the cross-sectional morphologies of each electrode were observed to check for thickness changes before (Fig. S23a–c) and after (Fig. S23d–f) battery evaluation. The thickness of all electrodes tested for 100 cycles increased primarily due to the volume expansion of Si. The thickness of the NBR-A electrode increased to 27 μ m after 100 cycles, compared to the pristine NBR-A electrode (22 μ m). In contrast, the thickness of the NBR-T (36 μ m) and NBR-X (33 μ m) electrodes increased significantly after 100 cycles, compared to the pristine

electrodes (25 µm for NBR-T and 21 µm for NBR-X), corresponding to increments of 44% and 57% for NBR-T and NBR-X, respectively (summarized in Fig. S24). Based on the results of thickness changes, it is clear that the extent of volume expansion during battery operation strongly depends on the mechanical properties of the electrodes, which are influenced by the binder materials. Therefore, solvent-binder compatibility can significantly affect the mechanical properties of the electrode, and this can be a critical factor in determining the electrochemical performance of volume-change materials during the charge-discharge process.

In solid-state batteries, applying a high stacking pressure of over 50 MPa is a common approach to ensure a well-connected Li⁺ pathway between solid particles. While this high pressure can enhance battery performance, lowering the stacking pressure to below 2 MPa, similar to the pressure used in commercial lithium-ion batteries, remains a significant challenge for the commercialization of solid-state batteries [35,36]. Therefore, it is crucial to identify an approach that effectively reduces the external pressure. To address this, we explored the correlation between the mechanical properties of the electrode and the external pressures in solid-state batteries. To confirm the effect of electrode mechanical properties on the external pressure in a solid-state battery system, the external pressure was adjusted to 16, 48, and 80 MPa. For this study, NBR-A and NBR-T electrodes were used to evaluate battery performance at different external pressures. Before measuring battery performance, the EIS analysis was carried out at different stack pressures. As seen in Fig. S25, the resistance of the bulk electrolyte does not appear to change due to the preapplied fabrication pressure of 480 MPa. By increasing the stack pressure up to 80 MPa for the NBR-A and NBR-T electrodes, each spectrum in the high-frequency regime (Transmission Line Model, TLM region), characterized by an approximately 40°-50° slope. becomes smaller, likely indicating the enhanced ionic conductivity in each electrode with increasing stack pressure of 80 MPa. Interestingly, the NBR-A binder electrode showed a higher resistance in the TLM region, likely due to the increased SE coverage ratio caused by the larger polymer domains, as discussed in Fig. S11.

At 80 MPa, both electrodes showed similar discharged capacities of \sim 510 mAh g⁻¹ with \sim 77% of initial coulombic efficiency

(ICE), likely due to the negligible impact of Si volume expansion caused by the enormous external pressure. However, at lower external pressures of 48 and 16 MPa, the NBR-A electrode exhibited higher capacity compared to the NBR-T electrode (Fig. 4a and b). At 48 and 16 MPa, the NBR-A electrode delivered 500 and 490 mAh g⁻¹, respectively, while the NBR-T electrode showed 440 and 390 mAh g⁻¹, respectively. Furthermore, it appears that the ICEs obtained at lower external pressures were also significantly affected by the mechanical properties of the electrodes. NBR-A electrodes maintained a high ICE of 77%, even at lower

external pressures. In contrast, the ICE for the NBR-T electrode dropped notably from 77% (at 80 MPa) to 59% (at 16 MPa). This suggests that the volume expansion of Si during the initial charge was not fully reversible in the subsequent discharge process, leading to the reduced ICE at lower stack pressures for the NBR-T electrode. To further investigate, we analyzed the capacity contribution of graphite (NG) and silicon (Si) active materials during the first discharging cycle. As shown in Fig. 4(d), the NG/Si discharge capacity ratio in the initial cycle varied depending on both the binder type and external pressure. For the NBR-A electrode, the

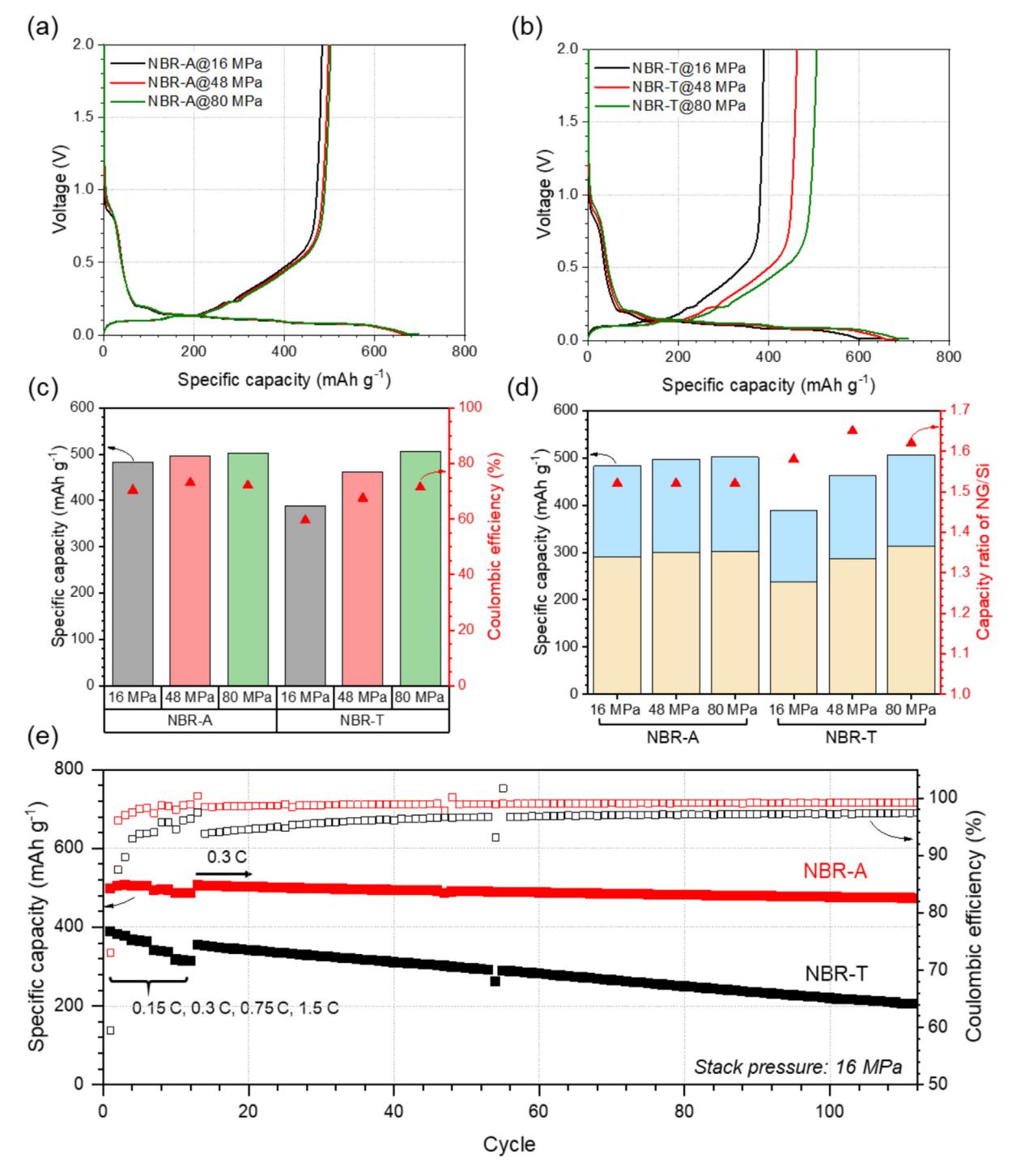


Fig. 4. (a, b) Charge-discharge voltage profiles of all solid-state NG-Si electrodes employing (a) NBR-A and (b) NBR-T at different stacking pressure at 16, 48, and 80 MPa with operating temperature of 60 °C. (c) Summary of the initial discharge capacity and coulombic efficiency obtained in panel (a and b). (d) Capacity contribution from NG and Si and their ratio in the first cycle. (e) Rate capability at 0.15, 0.3, 0.75, and 1.5C and consecutive cycle test for 100 cycles at 0.3C (Filled symbols: capacity, Empty symbols: coulombic efficiency) at stacking pressure of 16 MPa with operating temperature of 60 °C.

NG/Si ratio was approximately 1.52, regardless of external pressure. In contrast, the NBR-T electrode showed a higher capacity ratio of NG/Si: 1.58, 1.68, and 1.62 at 16, 48, and 80 MPa, respectively. This indicates that the mechanical properties of the electrode play an important role in maintaining the internal structure of the solid-state electrode during the charge-discharge process. Considering the volume expansion issues of silicon, the structural deformation of the electrode becomes more problematic under low stack pressure during battery operation. The changes in Si volume during the Li-Si alloying step directly affect the NG/Si electrode structure, with little compensation from the weak external pressure. Significant pulverization of Si can destroy electrode structure and form void spaces in the electrode, leading to deformation of the electronic and lithium ionic pathways to graphite, occurring at a slightly lower potential ($\sim 0.1 \text{ V vs. Li}^{+/0}$) than the Li-Si alloy formation potential ($\sim 0.4 \text{ V vs. Li}^{+/0}$). This can lead to a loss of graphite activity and a reduced specific capacity at lower stack pressure. However, when high stack pressure is applied, the structural stability of the NG/Si electrode is further enhanced by the external pressure, helping to maintain percolation between particles, which increases the capacity from graphite. Consequently, percolation between the solid particles (graphite, silicon, and solid electrolyte) in the electrode is well maintained due to the enhanced mechanical properties from solvent-induced polar interactions, and also this facilitates the charge-discharge performance of the graphite/Si composite electrode while minimizing capacity loss due to electrode structure degradation, even at low external pressure. Therefore, it is confirmed that the careful selection of a polymeric binder can positively affect the performance of solid-state batteries under lower external pressures.

To explore battery performance at low external pressure (16 MPa), composite electrodes with NBR-A or NBR-T were evaluated at different C-rates (0.15, 0.3, 0.75, and 1.5 C) for 3 cycles each, followed by a cyclability test at 0.3 C over 100 cycles. Even at a low external pressure of 16 MPa, the NBR-A electrode exhibited excellent rate capability at 1.5 C, similar to the performance at 48 MPa (Fig. 3e). In contrast, the NBR-T electrode showed poorer rate capability with 81% of retention at 1.5 C (compared to ~90% of capacity retention at the same C-rate under 48 MPa). For the cyclability test at 0.3 C, the NBR-A electrode displayed superior capacity retention of 93.0% after 100 cycles. Meanwhile, the NBR-T electrode showed a continuous decrease in capacity over cycles, resulting in 58% of capacity retention after 100 cycles. Over 100 cycles, the NBR-T electrode exhibited a lower average coulombic efficiency (~96%) than the NBR-A electrode (~99.0%), likely due to continuous electrode structural deformation caused by the poorer mechanical properties of the NBR-T binder.

The increased internal resistance in the NBR-T electrode was confirmed by EIS conducted after the cycle test. As shown in the EIS spectra (Fig. S26), the first semicircle, which corresponds to the interfacial resistance of the electrode, was much larger for the NBR-T electrode compared to the NBR-A electrode.

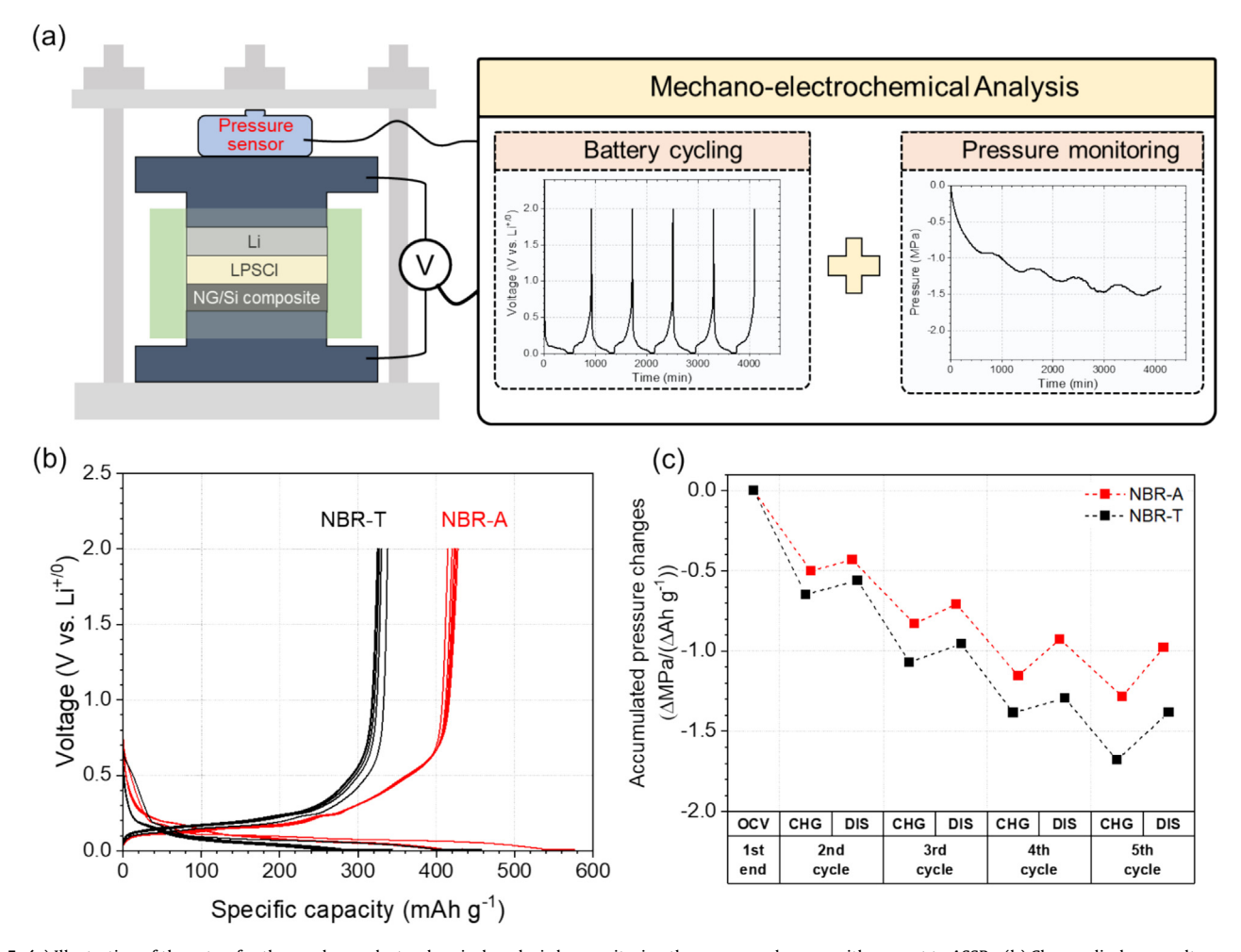


Fig. 5. (a) Illustration of the setup for the mechano-electrochemical analysis by monitoring the pressure changes with respect to ASSBs. (b) Charge-discharge voltage profiles of all solid-state NG-Si electrodes employing NBR-A (red) and NBR-T (black) over the initial consecutive 5 cycles. (c) Accumulated pressure changes with respect to the charge-discharge steps at each cycle. For the mechano-electrochemical analysis, all experiments were carried out with a stacking pressure of 30 MPa at 17 °C.

Additionally, the bulk resistance of the NBR-T electrode was slightly higher than that of the NBR-A electrode, likely due to the destructed interface between the electrode and the LPSCI SE layer caused by the continuous volume expansion of the NBR-T electrode.

It is well-known that maintaining an intimate solid-solid interface throughout the charge-discharge cycles is crucial for prolonging the performance of all-solid-state batteries, as it provides a continuous pathway for Li+. If any voids or cracks develop in the electrode during operation, these defects can hinder Li⁺ transfer. This issue is particularly important for alloying-type anode materials like silicon, which experiences significant volume expansion during the formation of Li-Si alloys, potentially disrupting the contact between particles [37,38]. To investigate the impact of the mechanical properties of the electrode on the performance of solid-state batteries, pressure changes in NBR-A and NBR-T electrodes were monitored while the battery was operated at 30 MPa, as shown in Fig. 5(a), under dry room conditions (dew point: < -60 °C, temperature: ~ 17 °C). To ensure stable electrochemical performance at 17 °C, the loading level of each electrode was intentionally reduced to approximately 1.8 mg cm⁻². As depicted in Fig. 5(c), the first five cycles of both NBR-A and NBR-T electrodes exhibited stable performance without capacity loss. The NBR-A electrode achieved a higher capacity of approximately 427 mAh g⁻¹, compared to 337 mAh g⁻¹ for the NBR-T electrode.

Pressure changes were monitored by cycling NG/Si composite

Pressure changes were monitored by cycling NG/Si composite electrodes made from NBR-A or NBR-T through five consecutive charge (lithiation) and discharge (delithiation) cycles. As shown in Fig. S27, the pressure changes were primarily governed by the volume changes of the Li metal counter electrode during the charge-discharge process [39,40]. During the charging phase, the pressure dropped due to the stripping of Li metal at the counter electrode, while during discharging, the pressure increased as Li was deposited back. Interestingly, the pressure monitored during

the discharge phase did not fully recover to its initial state, which could be due to irreversible reactions, such as void or crack formation from silicon volume expansion, or the formation of the SEI layer due to electrochemical side reactions between LPSCI and active materials. As mentioned earlier, crack or void formation induced by accumulated internal stress during battery operation is directly linked to performance degradation by increasing electrode resistance. To monitor the internal pressure changes during the charge-discharge process, the differences in pressure changes were normalized with respect to the charge or discharge capacity at each cycle. The cumulative pressure change over the first five cycles is shown in Fig. 5(c). In the first cycle, the internal pressure of both cells notably dropped during the initial lithiation step, and the pressure was not recovered during the subsequent delithiation step (Fig. S27b). This was likely due to Li⁺ consumption for SEI layer formation, which hindered the pressure recovery to its initial state. While the pressure drop during the first lithiation step was significantly higher in the NBR-T sample compared to the NBR-A electrode, the recovery pressure during delithiation was almost negligible for both electrodes. This phenomenon was complicated to interpret precisely due to the complex reactions involved, including SEI formation and crack/void formation from volume expansion in both the working and counter electrodes. Therefore, pressure monitoring was conducted starting from the second cycle. As shown in Fig. 5(c), both electrodes exhibited a trend of decreasing pressure over the cycles, but the accumulated pressure change in NBR-A was much lower than that in the NBR-T electrode. This may suggest that the higher binding strength of NBR-A could help stabilize the electrode structure by densifying the electrode during the initial cycles. In contrast, the NBR-T electrode was unable to provide sufficient adhesion, leading to a further decrease in pressure over cycles, likely due to the formation of internal voids caused by Si volume changes (as illustrated in Fig. 6).

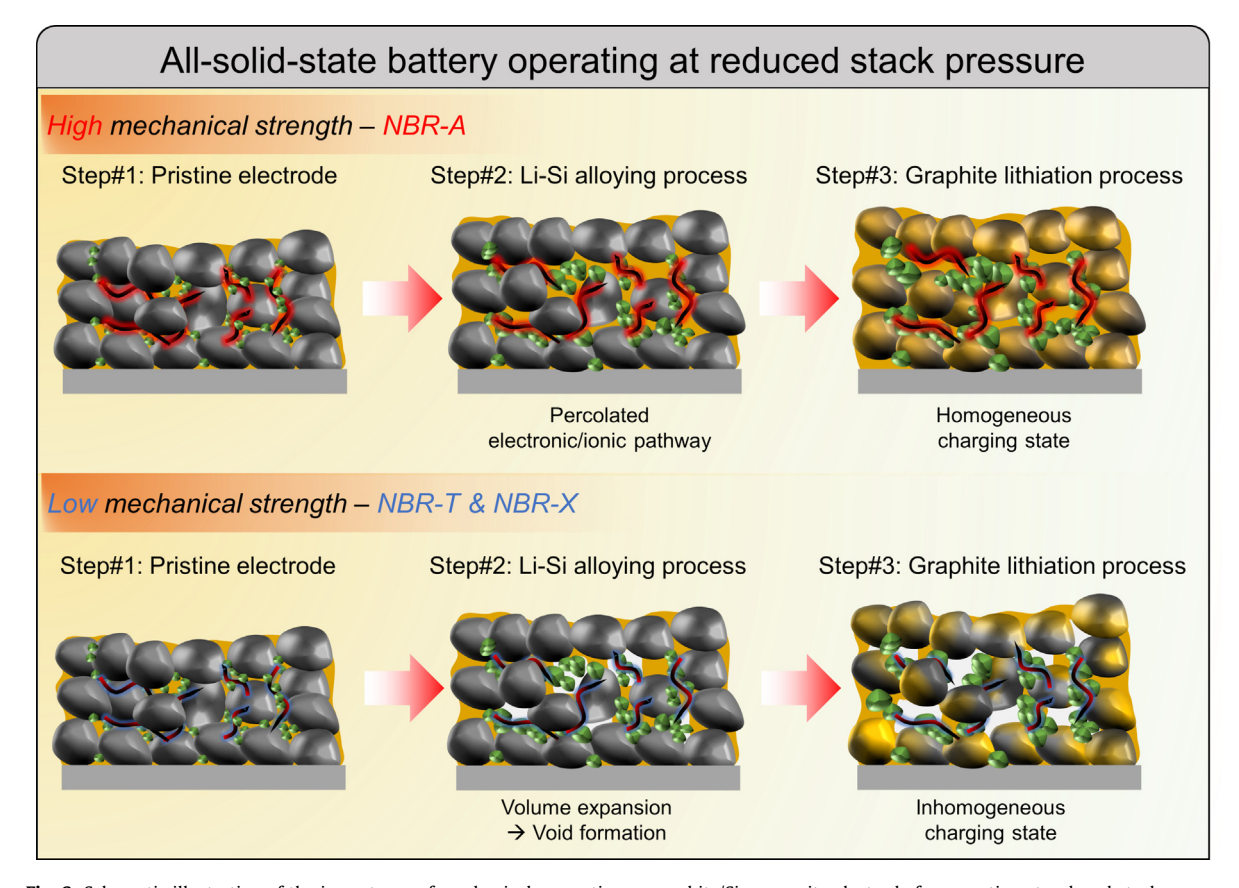


Fig. 6. Schematic illustration of the importance of mechanical properties on graphite/Si composite electrode for operating at reduced stack pressure.

4. Conclusions

In this work, we investigated the effect of solvent-induced polar interactions on nitrile binders for graphite-silicon anodes in ASSBs with sulfide-based solid electrolytes. NBR binders were dissolved in anisole, toluene, and p-xylene to fabricate electrodes, which were then analyzed for adhesion strength, cohesion, and electrochemical performance. The results showed that electrodes with NBR-A binder exhibited superior mechanical properties, including higher adhesion strength and cohesion compared to the other binder systems. This contributed to better electrochemical performance by effectively mitigating the structural damage caused by silicon volume expansion during cycling. Additionally, even at low external pressure (16 MPa), the NBR-A electrode maintained good performance, highlighting the importance of mechanical properties in maintaining battery performance under reduced pressure conditions. Further investigation of the pressure changes during battery operation revealed that the NBR-A electrode showed lower pressure variations compared to the NBR-T electrode. This indicates that NBR-A binder helps maintain the electrode structure against volume expansion of silicon, which contributes to better battery performance, especially at lower external pressure. The NBR-A electrode also exhibited better capacity retention and higher coulombic efficiency, further supporting the role of binder mechanical properties in improving solid-state battery performance under low-pressure conditions. Therefore, this work demonstrated that the compatibility between solvent and polymeric binder must be carefully considered based on their molecular structures and chemical properties, and this work also offered a potential solution for reducing the operating pressure of ASSBs.

CRediT authorship contribution statement

Jaecheol Choi: Writing – review & editing, Writing – original draft, Visualization, Validation, Supervision, Methodology, Investigation, Formal analysis, Conceptualization. Cheol Bak: Writing – review & editing, Writing – original draft, Visualization, Validation, Methodology, Investigation, Formal analysis, Conceptualization. Ju Young Kim: Validation, Investigation, Formal analysis. Dong Ok Shin: Validation, Formal analysis. Seok Hun Kang: Validation, Formal analysis. Yong Min Lee: Writing – review & editing, Supervision, Project administration, Funding acquisition. Young-Gi Lee: Writing – review & editing, Project administration, Funding acquisition.

Declaration of competing interest

The authors declare that they have no known competing financial interests or personal relationships that could have appeared to influence the work reported in this paper.

Acknowledgments

This work was supported by the Technology Innovation Program (00404166, Development of thin-film coating current collector and aqueous binder to enhance the adhesion and conductivity properties on the silicon-rich anode) funded By the Ministry of Trade, Industry & Energy(MOTIE, Korea), the National Research Council of Science & Technology(NST) grant by the Korea government (MSIT) (No. 2710024139), and the Institute of Civil Military Technology Cooperation funded by the Defense Acquisition Program Administration and Ministry of Trade, Industry and Energy of Korean government under grant No. 22-CM-FC-20.

Appendix A. Supplementary material

Supplementary data to this article can be found online at https://doi.org/10.1016/j.jechem.2025.02.012.

References

- [1] J.W. Choi, D. Aurbach, Nat. Rev. Mater. 1 (2016) 1-16.
- [2] X. Zeng, M. Li, D. Abd El-Hady, W. Alshitari, A.S. Ál-Bogami, J. Lu, K. Amine, Adv. Energy Mater. 9 (2019) 1900161.
- [3] M. Zhang, J. Xiao, W. Tang, Y. He, P. Tan, M. Haranczyk, D.Y. Wang, Adv. Energy Mater. 14 (2024) 2401241.
- [4] R. Gond, W. van Ekeren, R. Mogensen, A.J. Naylor, R. Younesi, Mater. Horiz. 8 (2021) 2913–2928.
- [5] K. Deng, Q. Zeng, D. Wang, Z. Liu, G. Wang, Z. Qiu, Y. Zhang, M. Xiao, Y. Meng, Energy Storage Mater. 32 (2020) 425–447.
- [6] Z. Zhang, Y. Shao, B. Lotsch, Y.-S. Hu, H. Li, J. Janek, L.F. Nazar, C.-W. Nan, J. Maier, M. Armand, Energy Environ. Sci. 11 (2018) 1945–1976.
- [7] Y. Xiao, Y. Wang, S.-H. Bo, J.C. Kim, L.J. Miara, G. Ceder, Nat. Rev. Mater. 5 (2020) 105–126.
- [8] L. Zhou, N. Minafra, W.G. Zeier, L.F. Nazar, Acc. Chem. Res. 54 (2021) 2717–2728.
- [9] Y. Nikodimos, C.-J. Huang, B.W. Taklu, W.-N. Su, B.J. Hwang, Energy Environ. Sci. 15 (2022) 991–1033.
- [10] V. Sharma, K. Singh, N. Krishnamurthy, Energy Adv. 3 (2024) 1222-1237.
- [11] K.H. Park, Q. Bai, D.H. Kim, D.Y. Oh, Y. Zhu, Y. Mo, Y.S. Jung, Adv. Energy Mater. 8 (2018) 1800035.
- [12] K.H. Park, D.Y. Oh, Y.E. Choi, Y.J. Nam, L. Han, J.Y. Kim, H. Xin, F. Lin, S.M. Oh, Y. S. Jung, Adv. Mater. 28 (2016) 1874–1883.
- [13] F.P. McGrogan, T. Swamy, S.R. Bishop, E. Eggleton, L. Porz, X. Chen, Y.M. Chiang, K.J. Van Vliet, Adv. Energy Mater. 7 (2017) 1602011.
- [14] G. Oh, M. Hirayama, O. Kwon, K. Suzuki, R. Kanno, Chem. Mater. 28 (2016) 2634–2640.
- [15] W. Zhang, T. Leichtweiß, S.P. Culver, R. Koerver, D. Das, D.A. Weber, W.G. Zeier, J.R. Janek, ACS Appl. Mater. Interfaces 9 (2017) 35888–35896.
- [16] K.T. Kim, D.Y. Oh, S. Jun, Y.B. Song, T.Y. Kwon, Y. Han, Y.S. Jung, Adv. Energy Mater. 11 (2021) 2003766.
- [17] D.Y. Oh, Y.J. Nam, K.H. Park, S.H. Jung, K.T. Kim, A.R. Ha, Y.S. Jung, Adv. Energy Mater. 9 (2019) 1802927.
- Mater. 9 (2019) 1802927. [18] C. Wang, J. Liang, Y. Zhao, M. Zheng, X. Li, X. Sun, Energy Environ. Sci. 14 (2021)
- 2577–2619. [19] D.Y. Oh, K.T. Kim, S.H. Jung, D.H. Kim, S. Jun, S. Jeoung, H.R. Moon, Y.S. Jung,
- Mater. Today 53 (2022) 7–15. [20] J. Choi, J.Y. Kim, S.H. Kang, D.O. Shin, M.J. Lee, Y.-G. Lee, J. Mater. Chem. A 12
- (2024) 6426–6437. [21] K. Lee, S. Kim, J. Park, S.H. Park, A. Coskun, D.S. Jung, W. Cho, J.W. Choi, J.
- Electrochem. Soc. 164 (2017) A2075.
 [22] D. Mackay, I. van Wesenbeeck, Environ. Sci. Technol. 48 (2014) 10259–10263
- [23] T. Ozturk, H.Y. Erbil, Coll. Surf. A 553 (2018) 327-336.
- [24] C. Liu, E. Bonaccurso, H.-J. Butt, Phys. Chem. Chem. Phys. 10 (2008) 7150-7157.
- [25] Y.J. Nam, S.-J. Cho, D.Y. Oh, J.-M. Lim, S.Y. Kim, J.H. Song, Y.-G. Lee, S.-Y. Lee, Y.S. Jung, Nano Lett. 15 (2015) 3317–3323.
- [26] D.H. Kim, D.Y. Oh, K.H. Park, Y.E. Choi, Y.J. Nam, H.A. Lee, S.-M. Lee, Y.S. Jung, Nano Lett. 17 (2017) 3013–3020.
- [27] Y. Shi, X. Zhou, G. Yu, Acc. Chem. Res. 50 (2017) 2642-2652.
- [28] H. Chen, M. Ling, L. Hencz, H.Y. Ling, G. Li, Z. Lin, G. Liu, S. Zhang, Chem. Rev. 118 (2018) 8936–8982.
- [29] Y.-J. Lee, S.-B. Hong, D.-W. Kim, J. Ind. Eng. Chem. 122 (2023) 341–348.
- [30] S. Schubert, J.T. Delaney Jr, U.S. Schubert, Soft Matter 7 (2011) 1581–1588.
- [31] D. Li, H. Liu, C. Wang, C. Yan, Q. Zhang, C.W. Nan, L.Z. Fan, Adv. Funct. Mater. (2024) 2315555.
- [32] B. Son, M.-H. Ryou, J. Choi, T. Lee, H.K. Yu, J.H. Kim, Y.M. Lee, ACS Appl. Mater. Interfaces 6 (2014) 526–531.
- [33] K. Kim, S. Byun, J. Choi, S. Hong, M.H. Ryou, Y.M. Lee, ChemPhysChem 19 (2018) 1627–1634.
- [34] J. Song, D.O. Shin, S. Byun, Y. Roh, C. Bak, J. Song, J. Choi, H. Lee, T.-S. Kwon, Y.-G. Lee, J. Electrochem. Sci. Technol. 13 (2022) 227–236.
- [35] J. Lee, T. Lee, K. Char, K.J. Kim, J.W. Choi, Acc. Chem. Res. 54 (2021) 3390–3402.
- [36] J. Oh, W.J. Chung, S.H. Jung, Y. Kim, Y. Lee, Y.J. Nam, S. Lee, C.H. Kim, J.W. Choi, Energy Storage Mater. 71 (2024) 103606.
 [37] J.Y. Kim, S. Jung, S.H. Kang, J. Park, M.J. Lee, D. Jin, D.O. Shin, Y.G. Lee, Y.M. Lee,
- Adv. Energy Mater. 12 (2022) 2103108.

 [38] D.H. Tan, Y.-T. Chen, H. Yang, W. Bao, B. Sreenarayanan, J.-M. Doux, W. Li, B. Lu,
- S.-Y. Ham, B. Sayahpour, Science 373 (2021) 1494–1499.
 [39] C. Lee, J.Y. Kim, K.Y. Bae, T. Kim, S.-J. Jung, S. Son, H.-W. Lee, Energy Storage
- Mater. 66 (2024) 103196. [40] S. Jun, Y.J. Nam, H. Kwak, K.T. Kim, D.Y. Oh, Y.S. Jung, Adv. Funct. Mater. 30 (2020) 2002535.